Correlation between photoluminescence and photoelectrochemical properties of SrHPO4/ BaHPO4/FTO anode material

Elhassan Amaterz, Abdessalam Bouddouch, Ahmed Tara, Aziz Taoufyq, Bahcine Bakiz, Abdeljalil Benlhachemi, Omar Jbara

Correlation between photoluminescence and photoelectrochemical properties of $SrHPO_4$/ $BaHPO_4$/FTO anode material

E. Amaterz [a,b,*], A. Bouddouch [a,c], A. Tara [b], A. Taoufyq [a], B. Bakiz [a], A. Benlhachemi [a], O. Jbara [b]

[a] Laboratoire Matériaux et Environnement (LME), Faculté des Sciences, Université Ibn Zohr, BP 8106, cité Dakhla, Agadir, Maroc.

[b] Institut de Thermique, Mécanique, Matériaux (ITheMM), Université de Reims Champagne-Ardenne, Reims, France.

[c] Institut Matériaux Microélectronique et Nanosciences de Provence, Université de Toulon, Aix Marseille Univ, CNRS, IM2NP, Toulon, France.

[*] Corresponding author: E-mail: elhassan.amaterz@etudiant.univ-reims.fr

Abstract

A new anode consisting of $BaHPO_4$/$SrHPO_4$ (SrP/BaP) micro-structured materials has been fabricated through two-step electrodeposition technique. Structural, vibrational, morphological, and optical properties of the anode films were investigated employing X-ray diffraction, Raman spectroscopy, scanning electron microscopy (SEM) and UV–Vis absorption spectroscopy, respectively. Photoluminescence (PL), and photo-electrocatalytic (PEC) activities of the samples were investigated and compared with those of the pure $BaHPO_4$ (BaP) and $SrHPO_4$ (SrP) samples. The PEC performance was of the order of 71 % within 25 min, which was less than both BaP (99%) and SrP (92%) in the same experimental conditions. These results reveal that BaP thin films combined with SrP microstructures remarkably changed the PL signals, and in turn significantly enhanced the PL activities, while the PEC has been lowered down. This was attributed to the photo-induced electron–hole pairs recombination as electrochemical impedance spectrum and photo-current response have shown. Based on these results, it is believed that the SrP/BaP film behaves as a sensitizer in the system and not as a photo-electrocatalyst.

Keywords

$SrHPO_4$/$BaHPO_4$; photo-electrocatalysis; photoluminescence; charge transfer; thin films.

1. Introduction

The luminescence spectrophotometry is a powerful tool for understanding the photo/electrocatalysis by studying the electronic structure, optical and photochemical properties of semiconductor materials. It is also used to obtain information about surface defects, oxygen vacancies, photo-induced charge carrier separation and recombination processes … etc. [1,2]. To understand the luminescence origin, it is important to keep in mind that the creation of electron-hole pairs within semiconductor materials generally leads to two extreme mechanisms. One is the recombination of these charge carriers while in the second case it is their efficient separation in a redox process, which occurs. The first mechanism is usually accompanied with a release of a certain amount of chemical energy which will further transform to heat or to light energy [1]. Theses latter result in a luminescence emission of the semiconductor material called PL phenomenon of the semiconductor. The second mechanism is usually beneficial for photocatalytic applications as the recombination of charge carriers will be retarded or even avoided, which improves the efficiency of the process [3,4]. However, in some cases, it was found that both photo/electrocatalytic activity and photoluminescence (PL) of semiconductor photocatalysts can increase likewise [5,6].

Recently, thanks to the increase in the development of science and technology, the inorganic semi-conductor materials with different morphologies and physico-chemical properties such as high surface areas, optical, electrical, and surface properties have shown a promising perspective in many fields, such as catalysis, coatings, and sensors [7–9]. Phosphate-based catalysts are one of the important classes of semiconductors which have been paid intense attention because of their excellent properties, such as the large band gap, high absorption of PO_4^{3-} in UV-Vis region, moderate phonon energy, high thermal as well as their high chemical stability. Therefore, they can be used in various applications such as supercapacitors, sensors, luminescence, Li-ion batteries, separation of radioactive ions, and photo/electrocatalysis [10–19] .

Among phosphate-based catalysts, strontium hydrogen phosphate ($SrHPO_4$) and barium hydrogen phosphate ($BaHPO_4$) have been investigated for a long time by many researchers as photocatalysts, surface conditioner, in batteries, fuel cells, proton conductor, for flame proofing, adsorption of heavy metals and dyes and thermal cathodes [20–25]. Thus, in view of

the above-mentioned studies on BaP and SrP based materials and their wide applications, it is thought worthwhile to study their composite material.

Because neither the PEC and PL properties of the $SrHPO_4/BaHPO_4$ composite nor the PL performance of $SrHPO_4$ and $BaHPO_4$ alone have not been studied, the correlation between the two properties as well, this paper is considered as a first attempt to study these properties.

For this reason, in the present work, we fabricated SrP/BaP by two-step electrochemical deposition for the first time to our knowledge. After a detailed morphological and structural characterization, the correlation between the photoluminescence (PL) and the photoelectrochemical properties was studied by measuring PL and PEC. The goal being to understand the suppressed radiative recombination and the charge separation of photogenerated carriers in the SrP/BaP films.

2. Materials and methods

2.1. Materials

Strontium (III) nitrate $Sr(NO_3)_2$, barium nitrate $Ba(NO_3)_2$, ammonium dihydrogen phosphate $(NH_4)H_2PO_4$, were provided from Fluka while Rhodamine B (RhB) was from Sigma–Aldrich. All these materials were used as received without further purification. F-doped SnO_2 (FTO) glass was purchased from SOLEMS S.A. France. Its sheet resistance is 6-8 Ω/square.

2.2. Preparation of BaP–SrP anode, PEC and PL procedures

The BaP–SrP anode was prepared by a two-step electrodeposition method on FTO substrates. Prior to the deposition, FTO substrates were ultrasonically cleaned in acetone, and deionized water, for 15 min sequentially. Firstly, an aqueous electrocatalytic solution composed by 0.03 M of strontium nitrate solution (50 mL) and 0.02 M of ammonium dihydrogen phosphate solution (50 mL) was prepared. The FTO substrates served as the working electrode, graphite rod was used as the counter electrode and the saturated calomel electrode (SCE) as the reference electrode. The electrodeposition procedure was performed at a temperature of 23°C and under a constant current density of −1 mA cm^{-2} relative to the counter electrode. Consequently, the electrochemical deposition of BaP on the SrP films was performed in an aqueous solution composed of 0.03 M of barium nitrate solution (50 mL) and 0.02 M of ammonium dihydrogen phosphate solution (50 mL). In this case the FTO/SrP films served as the working electrode. The applied current density was controlled at −0.5 mA cm^{-2} vs the counter electrode. The deposition procedure is illustrated in figure 1 below.

Figure 1: Schematic diagram of the deposition procedure of the SrP/BaP films.

The PEC degradation was carried out using the Rhodamine B as a model dye [20,26,27]. The process was achieved in an electrochemical cell consisting of three electrodes, SrP-BaP film as the photoanode, ECS as a reference electrode while the counter electrode was a carbon graphite. The reaction solution (100 mL) contains RhB solution and NaCl as supporting electrolyte. Samples are collected at specific time intervals for the determination of residual RhB concentration. The UV light source was a Xenon lamp (250 W).

The color removal efficiency was calculated according to the following equation:

$$\% \text{ color removal} = 100 \times ((C_0-C_t)/C_0) \quad (1)$$

Where C_0 and C_t are the concentration of RhB solution before the electrolysis and at each time "t" during the electrolysis, respectively.

The photoluminescence experiments were performed by using a Horiba JobinYvon LabRam HR800 spectrometer. This later is equipped with an argon-ionized laser as a source of excitation with a wavelength of 633 nm (1.95 eV) and whose power was fixed at 5µW. The control and acquisition of spectra was achieved using LabSpec software. The measurements were recorded in the spectral range between 400 and 1200 nm with an acquisition time of the spectra of 5 seconds.

2.3. Characterization

X-ray diffraction (XRD) using Bruker D8 Advance Twin diffractometer ($\lambda_{Cu\text{-}K\alpha}$ =0.154 nm) and Raman spectroscopy (Horiba Jobin-Yvon HR800 LabRam system) were used for SrP-BaP thin films structural analysis while Jeol JSM-6460LAV SEM operating at 20kV and equipped with an energy-dispersive X-ray spectrometer (EDS) was used to determine the morphology and the chemical composition of these films. UV-Visible spectrophotometry was employed to analyze the optical and pho-electrocatalytic behavior of SrP-BaP thin films.

2.4. Experimental design

Optimization experiments were carried out using response surface methodology (RSM), and in particular Central Composite Design (CCD) in which four factors were optimized [28]. The

experimental factors studied are initial NaCl concentration (X_1), applied current density (X_2), initial RhB concentration (X_3) and reaction time (X_4). These factors were varied over five levels between -α and + α at the determined ranges (Table SI 1). Based on the preliminary experiments and the experimental set-up, the choice of factors and their values were determined. The experimental data were fitted to second-order polynomial model according to the following equations:

$$N=2^k+2k+N_o \quad (2)$$

$$Y = b_0 + \sum_{i=1}^{n} b_i X_i + \sum_{i=1}^{n} b_{ii} X_i^2 + \sum_{i=1}^{n-1} \sum_{j=i+1}^{n} b_{ij} X_i X_j \quad (3)$$

Where N is the total number of experiments, k is the number of parameters and N_o is the number of central points. Y is the degradation efficiency of RhB; X_i and X_j are coded values of the factors (i and j range from 1 to k); b_0 is the intercept coefficient of model; b_j, b_{ii}, and b_{ij} are interaction coefficients of linear, quadratic, and the second-order terms, respectively; n is the number of independent parameters (n=4 in this study).

The analysis of variance (ANOVA) was performed in order to determine the individual linear, quadratic and interaction regression coefficient, this was performed using NONEMROD 2007 software. The quality of the fit of polynomial model was expressed by the value of correlation coefficient (R^2) and adjusted coefficient of determination (R^2_{adj}) as well as the ANOVA results [28].

3. Results and discussion

3.1. X-ray diffraction and Raman analysis

The XRD patterns were recorded to confirm the structure, phase and crystallinity of SrP-BaP as shown in Fig. 2.a The β-$SrHPO_4$ hexagonal phase is observed which is in well agreement with the JCPDS file no. 12-0368 (labeled as "●"). The XRD peaks for $BaHPO_4$ match the standard peak value with the orthorhombic phase of $BaHPO_4$ (JCPDS file no. 01-072-1370) (labeled as "∗"). It is worth to mention that BaP patterns are relatively more intense than those of SrP which is obvious because the BaP was deposited on SrP. BaP also filled the pores that may be present during the formation of SrP. The detected additional peaks correspond to the standard FTO peaks. It is noteworthy that no other diffraction peaks were observed. This confirms the synthesis of the SrP/BaP without any impurities.

The Raman spectrum is shown in Figure 2.b which is composed of the following wavenumbers. The bands at 1055 and 982 cm^{-1} are assigned to antisymmetric

stretching internal modes of the phosphate internal modes (ν_3 (A1g +Eg)), while the band at 943 cm^{-1} for symmetric stretching of P-O (ν_1 (A1g)). The two bands located at 580 and 533 cm^{-1} are due to the deformation bending of O-P-O (ν_4 (A1g + Eg)), while the intense band at 401 cm^{-1} is attributed to the bending vibration (ν_2 (Eg)). The external modes deriving from the vibrations of PO_4 , Sr-O and Ba–O at 207, 145 and 105 cm^{-1} [29,30] . The Raman results further confirmed the formation of SrP/BaP anode material.

Figure 2: a) The X-ray diffraction patterns of FTO substrate and SrP/BaP b) Raman spectrum of SrP/BaP anode material.

3.2. SEM and EDS analysis

Figure 3 presents the SEM images of SrP (a), BaP (c and SrP-BaP (b), it is clear that all of the films possess homogeneous surface morphology and without cracks. SrP shows flower-like morphology with the average diameter of flowers in the range of 10 μm while BaP shows a parallelepiped morphology with the diameter and length in the range of 4 μm and 16 μm, respectively. Additionally, the surface of SrP-BaP films was rougher than both the SrP and BaP films surface. We inferred that the formation of granular structure on the surface of film should be responsible for the increase of roughness since there is a slight agglomeration by mixtures of both SrP and BaP particles when BaP particles were introduced.

Energy-dispersive spectrometry (EDS) analysis of SrP-BaP was performed to further confirm the elemental analysis. As shown in table 1, the exclusive occurrence of the Sr, Ba, O, and P elements suggested the high purity of the films.

It is worth to mention that the areas delimited in the figure 4.c do not correspond to the given images of SrP (in figure 4.a) and BaP (in figure 4.c) but for the objective to show the existence of the two observed morphologies.

Figure 3: SEM images of (a) SrP, (b) SrP/BaP and (c) BaP thin films

Table 1: EDS analysis of SrP-BaP thin films

3.3. Optical properties and conductivity type

UV–vis diffuse reflectance spectroscopy for the synthesized samples was performed to monitor the optical response of the synthesized SrP-BaP thin film. The results are shown in Fig. 4a. The optical band gap energy was calculated by Tauc plots of $(\alpha h\upsilon)^2$ versus $h\upsilon$ [31,32], the estimated band gap of the obtained films was found to be 3.85 eV. The results were in a good agreement with literature data [25,33].

The Mott-Schottky analysis was performed to identify the type of conductivity for SrP/BaP (Fig.4b). Indeed, linear region of $1/C^2$ (C is the capacitance) relative to the applied potential was fitted with the Mott-Schottky equation. The positive slope of the line suggests n-type conductivity of SrP/BaP anode [34]. The corresponding intercept to the *x*-axis provides the flat-band potential, which can be taken as a reference for Fermi level of the semiconductor.

Figure 4: a) Estimation of band gap energy, b) conductivity type of the SrP/BaP anode film.

3.4. Experimental design and data analysis

Table SI-2 presents the conditions of 30 experimental runs, and the experimental response in terms of RhB degradation efficiency. According to the data in Table SI-2 and SI-3, the experimental design for % degradation of RhB in terms of coded factors was modelled by a second-order polynomial equation given below (Eq. 4):

$$\%, \text{Degradation rate of RhB} = 229.27 - 23.72\,X_1 - 14.23\,X_2 - 30.83\,X_3 + 45.85\,X_4 - 42.89\,X_1^2 - 37.82\,X_2^2 - 30.21\,X_3^2 - 30.21\,X_4^2 + 0.97\,X_1X_2 + 7.75\,X_1X_3 + 7.75\,X_1X_4 - 0.97\,X_2X_3 + 0.97\,X_2X_4 - 17.43\,X_3X_4 \quad (4).$$

Results from the CCD experiments and the surface response counter plots in figure SI-1 and Table SI-3, the degradation of RhB depends on all the four studied variables, the linear terms and the quadratic terms having either negative or positive effects. However, the interaction of NaCl concentration and applied current density, the initial dye concentration and the applied current density are not significant as *p*-value for all these two terms is greater than 0.05. All the other terms are significant as *p*-values for them are less than 0.05% [35]. However, the non-significant terms were not eliminated from the model because it would reduce the dimensionality and thus the accuracy of the response surface. Based on the values of independent variables coefficients in the regression model, the order in which the studied

variables affect the response as follows: reaction time (X_4) > RhB initial concentration (X_3) > initial NaCl concentration (X_1) > applied current density (X_2).

Finally, to test the significance of the model, the ANOVA was carried out and the obtained results are given in Table SI-3. A very low probability value ($P_{model} < 0.0001$) indicated that the model obtained was highly significant [36]. Furthermore, the R^2 test has been also used for the validation of the mathematical model. The R^2 of the quadratic model was 0.94. Adjusted R^2 (Adj-R^2), which is also a measure of goodness of a fit, was 0.89, indicating a satisfactory adjustment of the polynomial model to the experimental data. The final validation of the experimental model of CCD is confirmed if the selected model provides adequate approximation of the real system. The correlation between experimental and predicted values in the optimal conditions is given in Table 2. Based on the obtained results, it can be concluded that there is a good agreement between the experimental and predicted values. The degradation rate of RhB was 54 %, which is in close approximation to the predicted value 52.8 %. The results show that the proposed model used in this study is a suitable and usable to describe the aqueous electrodegradation of RhB onto SrP/BaP electrodes.

Table 2: Optimum values of the factors studied for optimal RhB degradation.

3.5. Photo-electrocatalytic properties

To investigate the PEC activity of SrP/BaP electrode, experiments using the optimal conditions found by the RSM (shown in Table 2) were performed and the obtained results are given in Fig. 5. Initially, the thin films were immersed in RhB dye solution in the dark for 60 minutes and the concentration of the dye was measured in order to achieve the adsorption of dye onto the electrode, the obtained results revealed that a very negligible decrease in the concentration of the dye was observed (1 %). The photolysis of RhB dye was also investigated and the concentration did not decrease, only 8% of degradation was obtained indicating the photostability of RhB dye during the reaction time of experiments. The photocatalysis experiment was conducted without applying a current density and after 25 min, 14 % of initial dye concentration was eliminated. The electrocatalysis experiment were performed by applying 13.6 $mA.cm^{-2}$ without light illumination; 54 % degradation efficiency was obtained. On the other hand, the UV light illumination with applying a current density have led to a superior degradation performance of the order of 71 % within 25 min. This

superior PEC activity can be attributed to the synergistic effect between photocatalysis and electrocatalysis.

To explain the synergic effect shown, when the SrP/BaP is subjected to an applied current density in combination with UV light, the separation of electrons-holes pairs is favored as the photogenerated electrons can travel easily from the working to the counter electrode via the external circuit. This also increases the amount of charge carriers being available in the system which therefore increases the number of active radicals and thus promotes the photoelectrodegradation efficiency.

However, comparing BaP and SrP PEC efficiencies in the same conditions, the SrP/BaP shows less performance as shown in figure 6. High recombination rates are believed to be behind the observed phenomena as it will be explained by photoluminescence and impedance studies, and thus limits the efficiency process.

Figure 5: Comparison of adsorption, photocatalysis, electrocatalysis and photo-electrocatalysis performances of SrP-BaP electrode. Experimental conditions: reaction time: 25 min, [NaCl]=0.18 M, current density = 13.6 $mA.cm^{-2}$, and [RhB]=6 M.

Figure 6: Comparison of PEC process of different electrodes under the same conditions.

3.6. PL spectra analysis

$SrHPO_4$ and $BaHPO_4$ are one kind of commonly used luminescent host materials. For example, $SrHPO_4$ doped with Eu^{3+}, Ce^{3+}, Tb^{3+} have shown important luminescent properties under the excitation of UV light [37]. However, these two materials have been doped with luminescent centers such as rare earth elements which are typically expensive. Thus, much effort should be devoted to explore self-activated luminescent materials that do not contain expensive elements. Therefore, the photoluminescence properties of SrP, BaP and SrP/BaP films have been investigated and shown in figure 7 below. The PL curves of pure SrP and pure BaP are measured with the same PL system and identical settings for the purpose of comparisons. BaP exhibits a broadband green emission from 350 to 800 nm and peaking around the wavelength of 522 nm. While SrP shows important luminescent properties than

$BaHPO_4$. Indeed, a broad emission band extending from 380 to 800 nm and peaking around 522 and 646 nm corresponding to green and red emissions, respectively, is observed. This broad band suggests that the emission process is typical of a multiphonon or multilevel process, i.e., a system in which the relaxation occurs by means of several paths and involving the participation of numerous states [38]. Compared to the pure BaP and SrP, the SrP/BaP film shows a great enhancement in its light emission indicating that the luminescence properties for the SrP/BaP are enhanced by BaP coating on SrP. This can be explained by the existence of larger number of defects of metal atom and oxygen vacancies, compared to BaP and SrP separately, during its crystal growth process [39].

Moreover, the higher recombination rate of photo-generated electrons and holes are also responsible for the luminescence. Indeed, the obtained results from PEC studies indicated that there was not charge carriers recombination suppression. Such results were reported elsewhere [40,41].

Figure 7: PL properties of the various films elaborated

3.7. EIS analysis and photo-current response

Using electrochemical impedance spectroscopy (EIS), Nyquist plots of BaP, SrP and SrP/BaP were carried out to give further evidence on the recombination rate. These plots are displayed in the figure 8a. All the three catalysts exhibit semicircles in the studied frequency region. The arc radius on the Nyquist plot of BaP is smaller than that of SrP, while that of SrP-BaP is bigger than those of SrP and BaP indicating that the charge transfer resistance is higher in the BaP/SrP film. This also indicated that a higher charge recombination and a less efficient charge separation were observed for the SrP/BaP films.

To shed more light on the separation efficiency of electrons and holes. Photocurrent measurement was used to investigate the excitation and transfer of photo-generated charge carriers in SrP/BaP anode material. In fact, the photocurrent is formed mainly by transferring photogenerated electrons, formed while exciting the photocatalyst by UV light, to the counter electrode; the higher photocurrent, usually of the order of Ampere, indicates more effective separation and longer lifetime of the photogenerated electrons. Figure 8b shows the photocurrent density versus the irradiation time curve of SrP/BaP samples under several on-

off illumination cycles. The photocurrent density obtained was almost 0.06 $\mu A.cm^{-2}$ indicating a higher recombination and a less efficient separation of photo-generated electron-hole pairs occurred at the interface between SrP and BaP in the SrP/BaP anode material.

Figure 8: a) Electrochemical impedance spectroscopy of SrP, BaP and SrP/BaP, b) Photo-current response of the SrP/BaP anode material.

Conclusion

In summary, SrP/BaP anode was synthesized using two-step electrodeposition. The study of optical properties has shown a band gap of 3.9 eV and n-type conductivity. The morphological study shows the presence of the BaP particles over the SrP flowers while XRD and EDS analysis have proved the existence of two phases without any impurities. The PEC activity towards RhB degradation has been optimized using RSM in combination with the CCD matrix. Although the synergic effect being generated by combining UV light with current density, SrP/BaP exhibits relatively high luminescence activity and less PEC performance in degrading RhB compared to pure BaP and SrP. The obtained results were explained by charge transfer process for the SrP/BaP thin films. It was found that the photogenerated charge carriers show high recombination rates as the photocurrent response had revealed. The EIS as well has shown that the composite is characterized by a high charge transfer resistance. Overall, the findings of this study revealed that SrP/BaP anode film can be used to fabricate optical devices especially high-efficiency green and red light-emitting devices.

Acknowledgements

This project was financially supported by CAMPUS FRANCE (PHC TOUBKAL 2018 (French-Morocco bilateral program) Grant Number: 38999WE) and PPR project number PPR/2015/32.

References

[1] J. Liqiang, Q. Yichun, W. Baiqi, L. Shudan, J. Baojiang, Y. Libin, F. Wei, F. Honggang, S. Jiazhong, Review of photoluminescence performance of nano-sized semiconductor materials and its relationships with photocatalytic activity, Sol. Energy

Mater. Sol. Cells. (2006). doi:10.1016/j.solmat.2005.11.007.

[2] B. Bakiz, A. Hallaoui, A. Taoufyq, A. Benlhachemi, F. Guinneton, S. Villain, M. Ezahri, J.C. Valmalette, M. Arab, J.R. Gavarri, Luminescent properties under X-ray excitation of Ba(1−x)PbxWO4 disordered solid solution, J. Solid State Chem. (2018). doi:10.1016/j.jssc.2017.10.014.

[3] M. Ni, M.K.H. Leung, D.Y.C. Leung, K. Sumathy, A review and recent developments in photocatalytic water-splitting using TiO2 for hydrogen production, Renew. Sustain. Energy Rev. (2007). doi:10.1016/j.rser.2005.01.009.

[4] X.Z. Li, F.B. Li, C.L. Yang, W.K. Ge, Photocatalytic activity of WOx-TiO2 under visible light irradiation, J. Photochem. Photobiol. A Chem. (2001). doi:10.1016/S1010-6030(01)00446-4.

[5] L. Jing, F. Yuan, H. Hou, B. Xin, W. Cai, H. Fu, Relationships of surface oxygen vacancies with photoluminescence and photocatalytic performance of ZnO nanoparticles, Sci. China, Ser. B Chem. (2005). doi:10.1360/03yb0191.

[6] J. Liqiang, S. Xiaojun, X. Baifu, W. Baiqi, C. Weimin, F. Honggang, The preparation and characterization of la doped TiO2 nanoparticles and their photocatalytic activity, J. Solid State Chem. (2004). doi:10.1016/j.jssc.2004.05.064.

[7] G.M. Lohar, J. V. Thombare, S.K. Shinde, S.H. Han, V.J. Fulari, Structural, photoluminescence and photoelectrochemical properties of electrosynthesized ZnSe spheres, J. Mater. Sci. Mater. Electron. (2014). doi:10.1007/s10854-014-1750-4.

[8] P. Singh, P. Shandilya, P. Raizada, A. Sudhaik, A. Rahmani-Sani, A. Hosseini-Bandegharaei, Review on various strategies for enhancing photocatalytic activity of graphene based nanocomposites for water purification, Arab. J. Chem. (2020). doi:10.1016/j.arabjc.2018.12.001.

[9] A. Amedlous, O. Amadine, Y. Essamlali, K. Daanoun, M. Aadil, M. Zahouily, Aqueous-phase catalytic hydroxylation of phenol with H2O2 by using a copper incorporated apatite nanocatalyst, RSC Adv. (2019). doi:10.1039/c9ra02021g.

[10] S. Vadivel, D. Maruthamani, M. Kumaravel, B. Saravanakumar, B. Paul, S.S. Dhar, K. Saravanakumar, V. Muthuraj, Supercapacitors studies on BiPO 4 nanoparticles synthesized via a simple microwave approach , J. Taibah Univ. Sci. (2016).

doi:10.1016/j.jtusci.2016.09.007.

[11] Z. Wang, J. Feng, M. Pang, S. Pan, H. Zhang, Multicolor and bright white upconversion luminescence from rice-shaped lanthanide doped BiPO4 submicron particles, Dalt. Trans. (2013). doi:10.1039/c3dt51010g.

[12] V.D. Nithya, R. Kalai Selvan, L. Vasylechko, Hexamethylenetetramine assisted hydrothermal synthesis of BiPO<inf>4</inf> and its electrochemical properties for supercapacitors, J. Phys. Chem. Solids. (2015). doi:10.1016/j.jpcs.2015.06.007.

[13] C. Pan, Y. Zhu, A review of BiPO4, a highly efficient oxyacid-type photocatalyst, used for environmental applications, Catal. Sci. Technol. (2015). doi:10.1039/c5cy00202h.

[14] T. Zeng, X. Yu, K.H. Ye, Z. Qiu, Y. Zhu, Y. Zhang, BiPO<inf>4</inf> film on ITO substrates for photoelectrocatalytic degradation, Inorg. Chem. Commun. (2015). doi:10.1016/j.inoche.2015.04.027.

[15] Z. Qiu, T. Zeng, K. Ye, X. Yu, Y. Zhu, Y. Zhang, Electrochemical Synthesis of Photoelectrocatalytic Thin Films of Hexagonal $BiPO_4$ Nanorods, J. Electrochem. Soc. 163 (2016) H18–H23. doi:10.1149/2.0111602jes.

[16] L. Herschke, J. Rottstegge, I. Lieberwirth, G. Wegner, Zinc phosphate as versatile material for potential biomedical applications Part 1, J. Mater. Sci. Mater. Med. (2006). doi:10.1007/s10856-006-6332-4.

[17] Y. Naciri, H. Ait Ahsaine, A. Chennah, A. Amedlous, A. Taoufyq, B. Bakiz, M. Ezahri, S. Villain, A. Benlhachemi, Facile synthesis, characterization and photocatalytic performance of Zn3(PO4)2platelets toward photodegradation of Rhodamine B dye, J. Environ. Chem. Eng. (2018). doi:10.1016/j.jece.2018.02.009.

[18] D.J. Martin, G. Liu, S.J.A. Moniz, Y. Bi, A.M. Beale, J. Ye, J. Tang, Efficient visible driven photocatalyst, silver phosphate: performance, understanding and perspective, Chem. Soc. Rev. (2015). doi:10.1039/c5cs00380f.

[19] A. Bouddouch, E. Amaterz, B. Bakiz, A. Taoufyq, S. Villain, J. Gavarri, M. Ezahri, A. Benlhachemi, G. Cedex, Role of thermal decomposition process in the photocatalytic or photoluminescence properties of BiPO 4 polymorphs., (n.d.) 0–1. doi:10.1002/wer.1340.

[20] E. Amaterz, A. Tara, A. Bouddouch, A. Taoufyq, B. Bakiz, F. Lazar, M. Gilliot, A.

Benlhachemi, L. Bazzi, O. Jbara, Hierarchical flower-like SrHPO4 electrodes for the photoelectrochemical degradation of Rhodamine B, J. Appl. Electrochem. (2020). doi:10.1007/s10800-020-01416-1.

[21] E. Amaterz, A. Bouddouch, A. Chennah, A. Tara, A. Taoufyq, B. Bakiz, F. Lazar, A. Benlhachemi, L. Bazzi, O. Jbara, Heat treatment effect on the structure and morphology of strontium monoacid orthophosphate thin films, Mater. Today Proc. (2019). doi:10.1016/j.matpr.2019.08.070.

[22] A. Fischer, T. Mallat, A. Baiker, Amination of diols and polyols to acyclic amines, Catal. Today. (1997). doi:10.1016/S0920-5861(97)00009-6.

[23] B. Louati, K. Guidara, M. Gargouri, M. Fourati, 1H NMR, 31P NMR and Raman Study of CaHPO4and SrHPO4, Zeitschrift Fur Naturforsch. - Sect. A J. Phys. Sci. (2005). doi:10.1515/zna-2005-1-220.

[24] S. V. Levchik, E.D. Weil, A review of recent progress in phosphorus-based flame retardants, J. Fire Sci. (2006). doi:10.1177/0734904106068426.

[25] F. Zhang, Y. Shi, Z. Zhao, W. Song, Y. Cheng, The photo-catalytic activities of MP (M = Ba, Ca, Cu, Sr, Ag; P = PO 43- , HPO 42-) microparticles, Appl. Surf. Sci. (2014). doi:10.1016/j.apsusc.2013.12.010.

[26] A. Bouddouch, E. Amaterz, B. Bakiz, A. Taoufyq, F. Guinneton, S. Villain, J.R. Gavarri, M. Ezahri, J.C. Valmalette, A. Benlhachemi, Role of thermal decomposition process in the photocatalytic or photoluminescence properties of BiPO4 polymorphs, Water Environ. Res. (2020) 0–1. doi:10.1002/wer.1340.

[27] A. Chennah, Y. Naciri, A. Taoufyq, B. Bakiz, L. Bazzi, F. Guinneton, S. Villain, J.R. Gavarri, A. Benlhachemi, Electrodeposited zinc phosphate hydrate electrodes for electrocatalytic applications, J. Appl. Electrochem. 0 (2018) 0. doi:10.1007/s10800-018-1261-8.

[28] Z. Anfar, H. Ait Ahsaine, M. Zbair, A. Amedlous, A. Ait El Fakir, A. Jada, N. El Alem, Recent trends on numerical investigations of response surface methodology for pollutants adsorption onto activated carbon materials: A review, Crit. Rev. Environ. Sci. Technol. (2019). doi:10.1080/10643389.2019.1642835.

[29] T. BenChaabane, L. Smiri, A. Bulou, Vibrational study and crystal structure refinement

of BaHPO4, Solid State Sci. (2004). doi:10.1016/j.solidstatesciences.2003.11.008.

[30] X.F. Wang, Q. Yang, G.G. Wang, X.Z. Wang, J.C. Han, A new single-component KCaY(PO 4) 2 :Dy 3+ , Eu 3+ nanosized phosphor with high color-rendering index and excellent thermal resistance for warm-white NUV-LED, RSC Adv. (2016). doi:10.1039/c6ra20912b.

[31] P. Zhu, J. Xu, M. Duan, R. Wang, L. Xie, M. Hu, P. Wang, Fabrication of a double Z-type g-C3N4/AgBr/Ag3PO4 composite with enhanced visible-light photocatalytic activity for organic dye elimination, Opt. Mater. (Amst). (2020). doi:10.1016/j.optmat.2020.110076.

[32] M. Zhang, C. Piao, D. Wang, Z. Liu, J. Liu, Z. Zhang, J. Wang, Y. Song, Fixed Z-scheme TiO2|Ti|WO3 composite film as recyclable and reusable photocatalyst for highly effective hydrogen production, Opt. Mater. (Amst). (2020). doi:10.1016/j.optmat.2019.109545.

[33] S.K. Arora, T.R. Trivedi, V.A. Patel, Optical absorption in BaHPO4 single crystals, Scr. Mater. (2002). doi:10.1016/S1359-6462(02)00260-9.

[34] N. Labchir, E. Amaterz, A. Hannour, A. Ait, A. Ihlal, M. Sajieddine, L. Umr, Highly Efficient Nanostructured CoFe 2 O 4 Thin Film Electrodes for Electrochemical Degradation of rhodamine B, (n.d.). doi:10.1002/wer.1272.

[35] S. Karimifard, M.R. Alavi Moghaddam, Application of response surface methodology in physicochemical removal of dyes from wastewater: A critical review, Sci. Total Environ. (2018). doi:10.1016/j.scitotenv.2018.05.355.

[36] V.A. Sakkas, M.A. Islam, C. Stalikas, T.A. Albanis, Photocatalytic degradation using design of experiments: A review and example of the Congo red degradation, J. Hazard. Mater. (2010). doi:10.1016/j.jhazmat.2009.10.050.

[37] M. Wang, B. Tian, D. Yue, W. Lu, M. Yu, C. Li, Q. Li, Z. Wang, Crystal structure, morphology and luminescent properties of rare earthion-doped SrHPO4nanomaterials, J. Rare Earths. (2015). doi:10.1016/S1002-0721(14)60426-9.

[38] E. Orhan, M. Anicete-Santos, M.A.M.A. Maurera, F.M. Pontes, C.O. Paiva-Santos, A.G. Souza, J.A. Varela, P.S. Pizani, E. Longo, Conditions giving rise to intense visible room temperature photoluminescence in SrWO4 thin films: The role of

disorder, Chem. Phys. (2005). doi:10.1016/j.chemphys.2004.11.013.

[39] Z.L. Ning, W.J. Li, C.Y. Sun, P. Che, Z.D. Chang, Synthesis and optical properties of zinc phosphate microspheres, Trans. Nonferrous Met. Soc. China (English Ed. (2013). doi:10.1016/S1003-6326(13)62516-9.

[40] W. Widiyastuti, I. Maula, S. Machmudah, T. Nurtono, S. Winardi, K. Okuyama, Photocatalytic Activity Inhibition by ZnO-SiO_2 Nanocomposites Synthesized by Sonochemical Method, Adv. Mater. Res. (2015). doi:10.4028/www.scientific.net/amr.1112.209.

[41] N. Hagura, T. Takeuchi, S. Takayama, F. Iskandar, K. Okuyama, Enhanced photoluminescence of ZnOSiO2 nanocomposite particles and the analyses of structure and composition, J. Lumin. (2011). doi:10.1016/j.jlumin.2010.09.039.

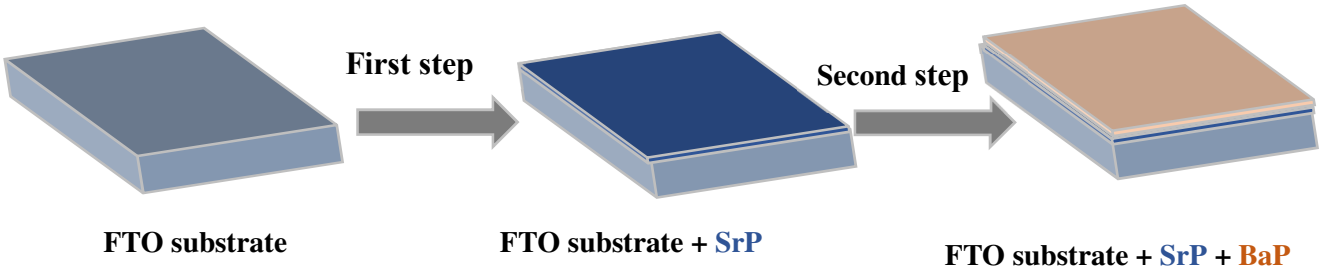

Figure 1: Schematic diagram of the deposition procedure of the SrP/BaP films.

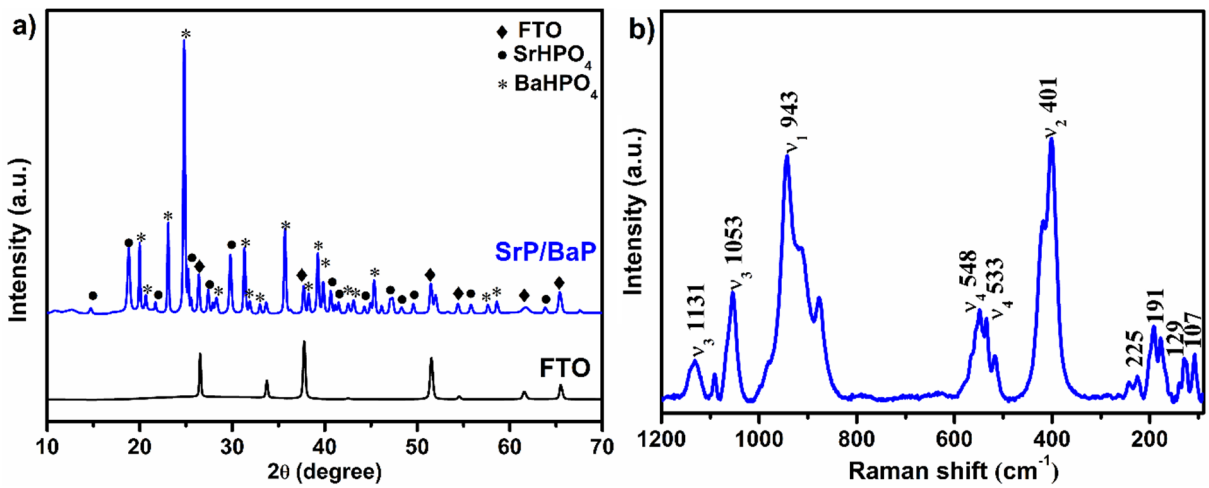

Figure 2: a) The X-ray diffraction patterns of FTO substrate and SrP/BaP b) Raman spectrum of SrP/BaP anode material.

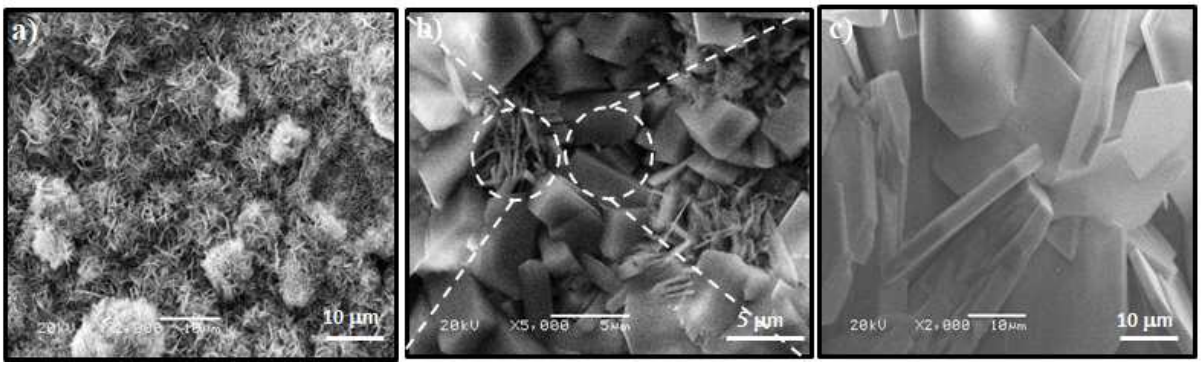

Figure 3: SEM images of (a) SrP, (b) SrP/BaP and (c) BaP thin films

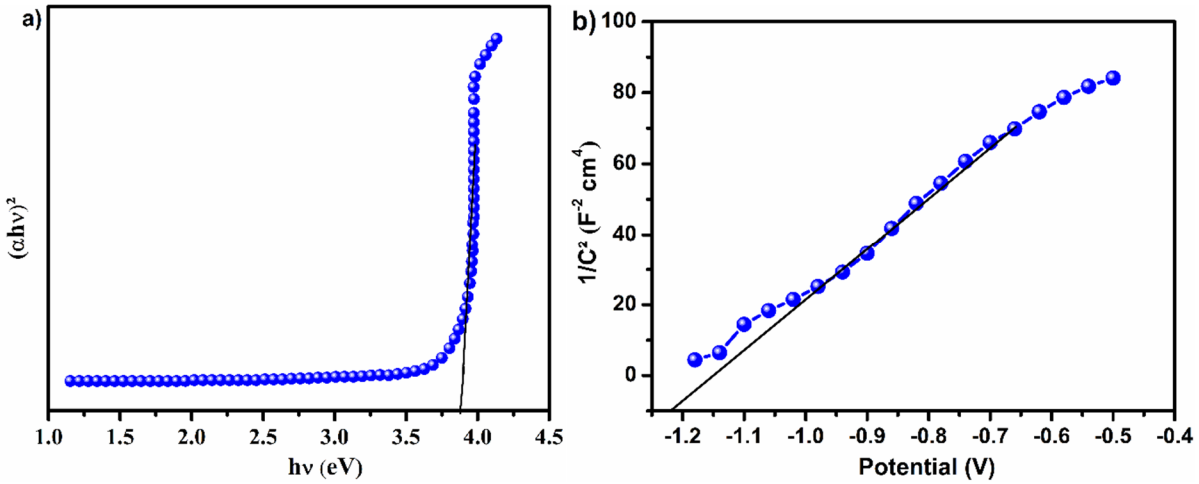

Figure 4: a) Estimation of band gap energy, b) conductivity type of the SrP/BaP anode film.

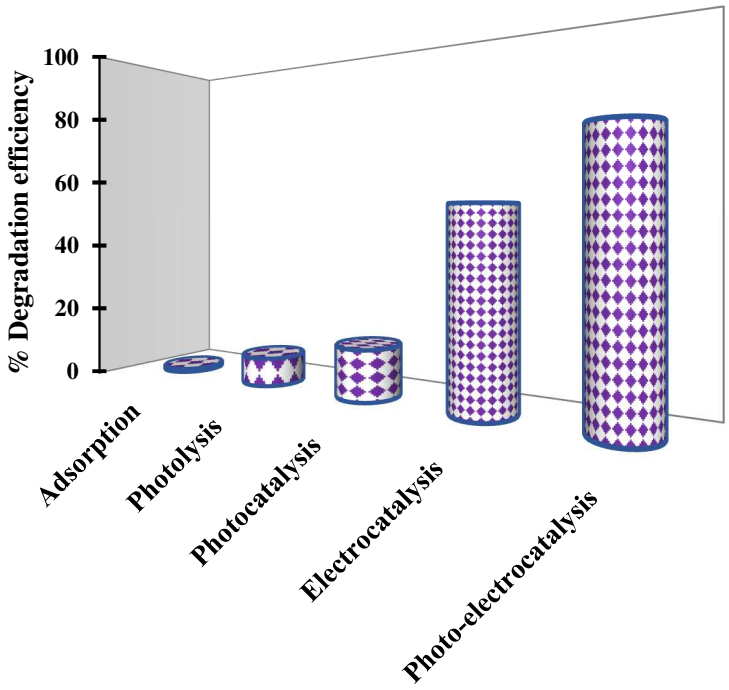

Figure 5: Comparison of adsorption, photocatalysis, electrocatalysis and photo-electrocatalysis performances of SrP-BaP electrode. Experimental conditions: reaction time: 25 min, [NaCl]=0.18 M, current density = 13.6 $mA.cm^{-2}$, and [RhB]=6 M.

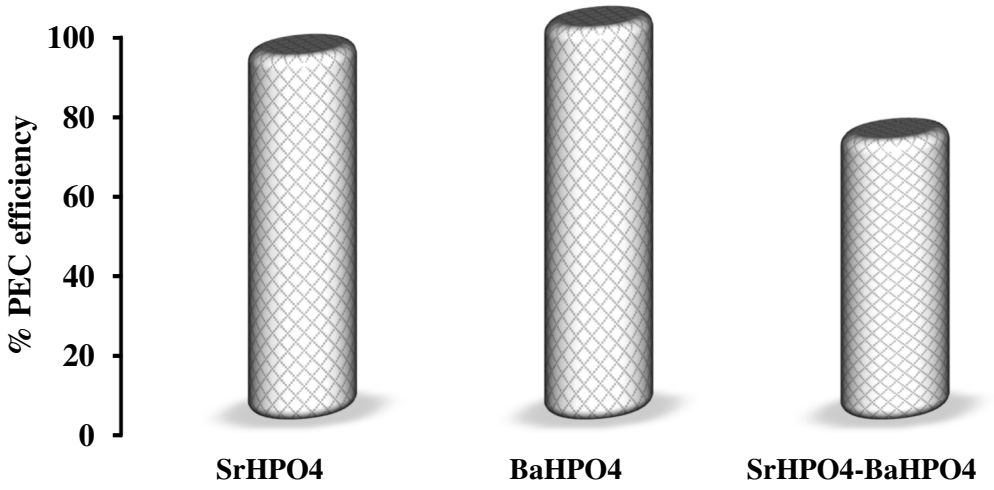

Figure 6: Comparison of PEC process of different electrodes under the same conditions.

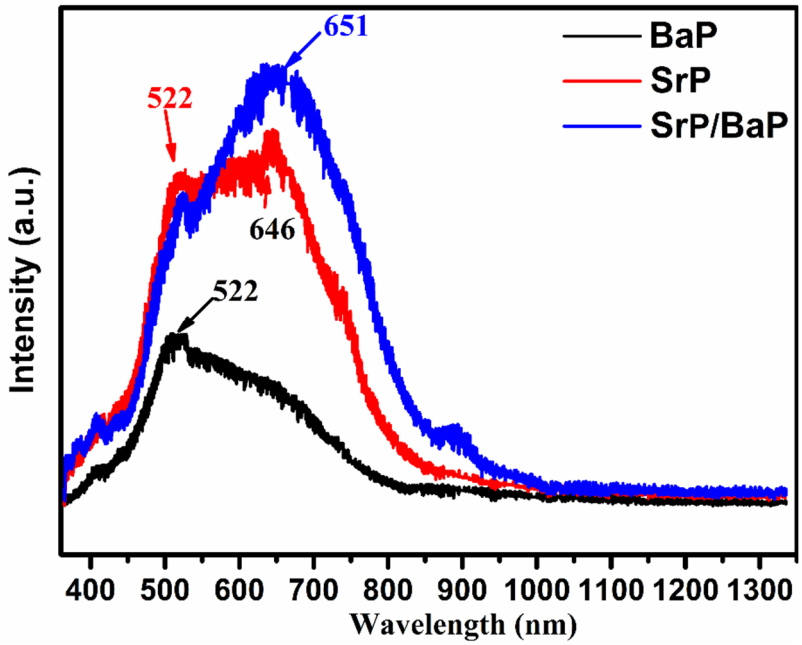

Figure 7: PL properties of the various films elaborated

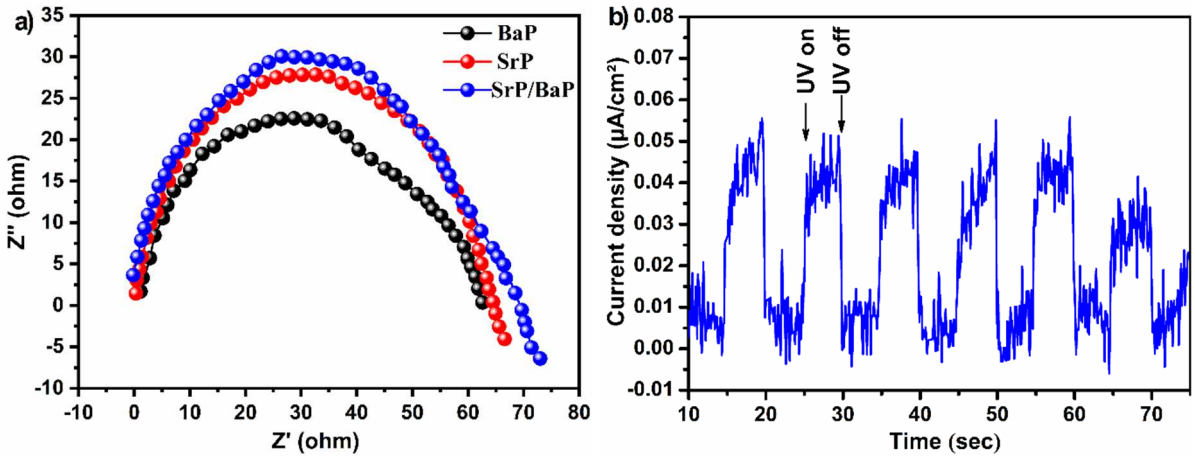

Figure 8: a) Electrochemical impedance spectroscopy of SrP, BaP and SrP/BaP, b) Photo-current response of the SrP/BaP anode material.

Table 1: EDS analysis of SrP-BaP thin films

Element	At%	mass%
O K	47.9	16.1
P K	23.5	15.4
Sr L	13.7	25.3
Ba L	14.9	43.2
Total	100.00	100.00

Table 2: Optimum values of the factors studied for optimal RhB degradation.

Factor	**Optimum values**	**Experimental Field**	
		% found by the model	% found by experience
[NaCl] (mol/l): $\mathbf{X_1}$	0.18	52.80 %	54 %
Current density (mA/cm²): $\mathbf{X_2}$	13.60		
[RhB_0] (mol/l): $\mathbf{X_3}$	6		
Time (min): $\mathbf{X_4}$	25.00		

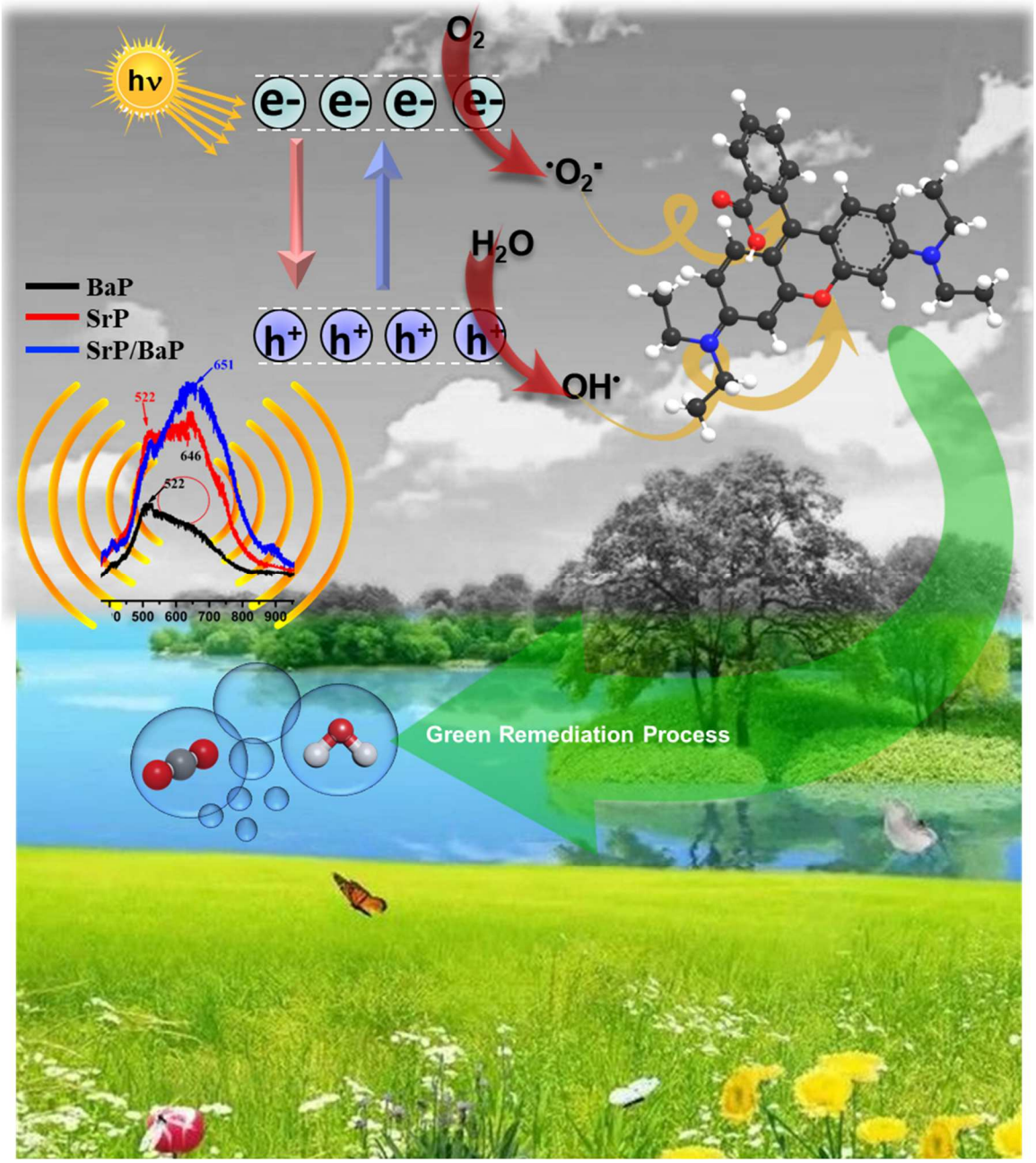
hν
e-
e-
e-
e-
O2
·O2-
H2O
OH·
h+
h+
h+
h+
BaP
SrP
SrP/BaP
651
522
646
522
0
500
600
700
800
900
Green Remediation Process